2017

Porous inclusions as hosts for phase change materials in cementitious composites: Characterization, thermal performance, and analytical models

Matthew Aguayo

Sumanta Das

See next page for additional authors

Authors
Matthew Aguayo, Sumanta Das, Cesar Castro, Nihat Kabay, Gaurav Sant, and Narayanan Neithalath

Porous inclusions as hosts for phase change materials in cementitious composites: Characterization, thermal performance, and analytical models

Matthew Aguayo[1], Sumanta Das[2], Cesar Castro[3], Nihat Kabay[4], Gaurav Sant[5], Narayanan Neithalath[6]

ABSTRACT

This paper examines the influence of four different lightweight aggregates (LWAs) having different pore structure features, on containing phase change materials (PCMs) within their pore network, and beneficially impacting the thermal properties of the mortar. The porosity and absorption capacity of the LWAs significantly influence the thermal conductivity. The incorporation of 5% of PCMs by total volume of the mortar reduces the composite thermal conductivity by 10% or more. Maxwell-Garnett effective medium and multi-step Mori-Tanaka mean-field homogenization models are employed to predict the composite thermal conductivity. Multi-step homogenization based either on known microstructural arrangement, or the property contrast between the constituent phases, are adopted. A microstructural contrast factor is defined, which accounts for both the thermal conductivities and the volume fractions of the phases with the highest property contrast. Smaller contrast factors indicate reduced divergence of the predictions from the experimental results, thereby aiding in the selection of suitable homogenization schemes for multi-phase composites.

Keywords: Phase Change Materials (PCMs), Microstructure, Lightweight Aggregate, Thermal Conductivity, Homogenization models

[1] Graduate student, School of Sustainable Engineering and the Built Environment, Arizona State University, Tempe AZ
[2] Assistant Professor, Department of Civil and Environmental Engineering, University of Rhode Island, Kingston, RI, United States
[3] Undergraduate Research Associate, School of Sustainable Engineering and the Built Environment, Arizona State University, Tempe AZ
[4] Associate Professor, Department of Civil Engineering, Yildiz Technical University, Istanbul, Turkey
[5] Associate Professor, Department of Civil and Environmental Engineering, University of California Los Angeles, Los Angeles, CA; Member, California Nanosystems Institute
[6] Professor, School of Sustainable Engineering and the Built Environment, Arizona State University, Tempe AZ, Corresponding Author; Narayanan.Neithalath@asu.edu; Phone: 001-480-965-6023; Fax: 001-480-965-0557

1. Introduction

Phase change materials (PCMs) are combined sensible-and-latent thermal energy storage (TES) materials that can be used to store and dissipate energy in the form of heat [1–4]. As the temperature increases, the endothermic phase change of PCMs from solid-to-liquid absorbs heat, while as the temperature decreases, the exothermic liquid-to-solid transition releases heat. The incorporation of PCMs in walls and roofs have been extensively studied as a means to reduce the energy consumption in passively designed buildings [5–8]. Several approaches to incorporate PCMs in concrete have been used, including the use of microencapsulated PCMs in powder form that can be added directly to concrete [9–11], or impregnation of liquid PCMs into porous inclusions to be used as aggregates in concrete [12–15].

This paper concerns the use of porous inclusions as carriers for PCMs in concrete. PCM in liquid state is impregnated into the pores of lightweight aggregates (LWAs). This overcomes one of the main disadvantages of lightweight structures as building envelopes, namely, the low thermal inertia. Large temperature fluctuations in such buildings can be reduced through the use of PCM incorporations, in addition to providing increased thermal insulation. Moreover, this approach can also be used for structural concretes in exposed conditions such as bridge decks to limit the number and/or intensity of freeze-thaw cycles experienced by concrete [16] and to reduce the rate of thermal deformation and stress development by controlling the temperature rise [17].

Several methods to impregnate porous aggregates with PCMs have been reported [18–20]. The amount of heat stored and released by PCMs contained within the pores of LWAs depends on the pore structure of the LWA as well as the thermal properties of the PCM (i.e., enthalpy, specific heat, and phase transition temperature). Thus a fundamental characterization of PCMs and LWAs is important in properly understanding their thermal response and the efficient design of LWA-PCM composite mortars. This paper evaluates four different types of LWAs with respect to their capacity to impregnate an organic paraffin-based PCM in their material structure, and consequently influence the composite thermal properties. These porous inclusions are incorporated into cement mortars and their thermal conductivities determined (using a guarded hot-plate method), ensuring that the volume fraction of PCM in all the mixtures remains the same. Effective medium and mean-field homogenization models are used to predict the thermal conductivity of the composite mortars. The dependence of predictive efficiency of the models on the relative volume fractions of microstructural phases of high property contrast, and the intensity of thermal property contrast is brought out.

2. EXPERIMENTAL PROGRAM

2.1. Materials

A commercially available Type I/II ordinary portland cement (OPC) conforming to ASTM C150, one bulk paraffin-based phase change material (PCM) supplied by Entropy Solutions (PureTemp 24X), and four different light weight aggregates (LWA) were used to proportion the mortars used in this study. The LWAs used were pumice (PU), perlite (PE), expanded shale/clay (ESC), and expanded slate (ES). Coarse sand (CS), having a median particle size of 600 µm was used in the control mortar. The particle size distributions of all the LWAs and the CS are shown in Figure 1, and the visual appearance of LWAs in Figure 2. The median particle size (d_{50}) of OPC was 10 µm and the median particle size for the LWAs ranged between 800 and 1200 µm.

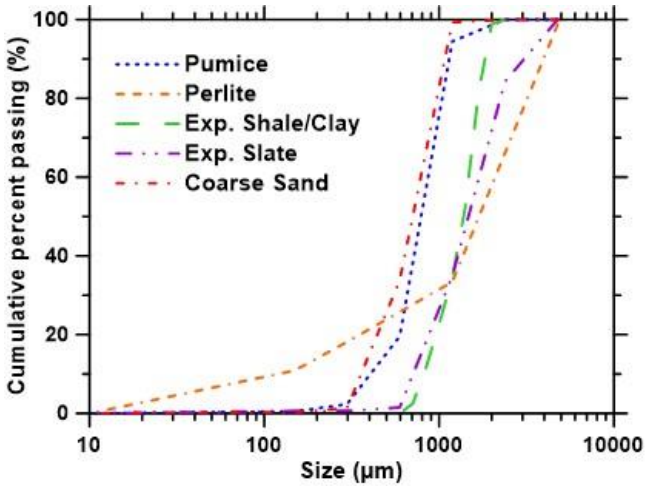

Figure 1: Particle size distributions of the LWAs and the coarse sand

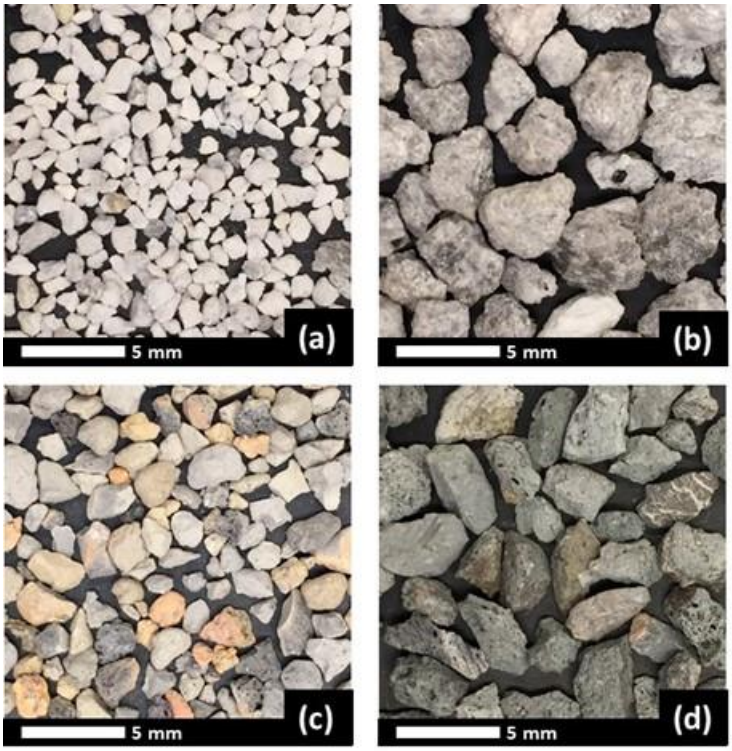

Figure 2: Lightweight aggregates used in this study: (a) pumice (PU), (b) perlite (PE), (c) expanded shale and clay (ESC), and (d) expanded slate (ES)

2.2 LWA Pretreatment and Absorption of PCM

LWAs are used as carriers for the PCMs in this study. Thus it is important to determine the absorption of PCM in each of the LWAs. The following procedure for pretreatment and absorption was implemented. Initially, LWA was washed and sieved to remove any material finer than 150 μm (No. 100 sieve), as their contribution to total absorption is deemed negligible. The use of finer material also likely results in erroneous absorption values because of the increased particle surface area that might cause the PCM to adsorb on the surfaces rather than absorbing into the pores. After washing the aggregates, they were placed in the oven at 100°C for 48 hours to remove any evaporable water and bring them to the oven dry (OD) condition. Drying beyond 48 hours resulted in negligible mass changes. The physical properties of the LWA including the relative densities in the oven dry and saturated surface dry conditions were measured in accordance with ASTM C128-15. The absorption of PCM into the pores of the LWA was determined by soaking a known mass of LWA in PureTemp 24X liquid for 24-to-72 hours, after which the soaked LWA was placed in a fine mesh to allow the excess PCM to drain. The soaking was performed at a temperature greater than the phase transition temperature of the PCM (in this case, 24°C) to keep it in the liquid state throughout. Vacuum saturation was not employed to ensure that the impregnation method can be easily replicated in practice. After 24 hours of draining, the soaked LWA was weighed

again, and the absorption was determined. Negligible increase in absorption was observed when the soaking time was increased beyond 72 hours, and thus the LWAs were soaked in liquid PCM for 72 hours and allowed to drain for 24 hours (to ensure saturated surface dry condition) prior to being mixed with the cement paste.

2.3 Mixtures

Ten mixtures (nine mortar, and one paste) were proportioned with a volumetric water-to-binder ratio, $(w/b)_v = 1.58$ (mass-based $w/p \approx 0.50$). Table 1 shows the mixture proportions and the corresponding nomenclature. The mortar samples were proportioned with a constant paste volume of 50%. The LWA mortars contained 50% LWA inclusions by volume. For the LWA mortars, 5% PCM by overall volume of the mortar was incorporated by adjusting the amount of LWA impregnated with the PCM, to be used in the mortar. This is illustrated in Figure 3(a) using the case of pumice aggregates as an example. The overall aim is to incorporate 5% of PCM by volume of the mortar. The pumice aggregate used in this study has a porosity of 39% and an absorption capacity of 21% (Section 3.1 provides more details on absorption). In other words, 21% of the total volume of LWAs will contain the PCM. If all the LWA (which is 50% by volume of the mortar) is saturated with PCM, then the volume fraction of PCM in the mortar is 21% of 50%, which is 10.5%. Since the intention is to use only 5% by volume of PCM in the mortar, PCM-soaked pumice LWAs will need to be used along with non-impregnated LWAs in this mortar. Thus, almost half of the total LWA used in this mortar will be non-impregnated ones. Alternatively, when perlite LWA with an absorption of 11.2% is considered as shown in Figure 3(b), almost all of the LWAs need to be impregnated to achieve the desired PCM volume fraction of 5% (the volume fraction of PCM in the mortar is 11.2% of 50%, which is 5.6%).

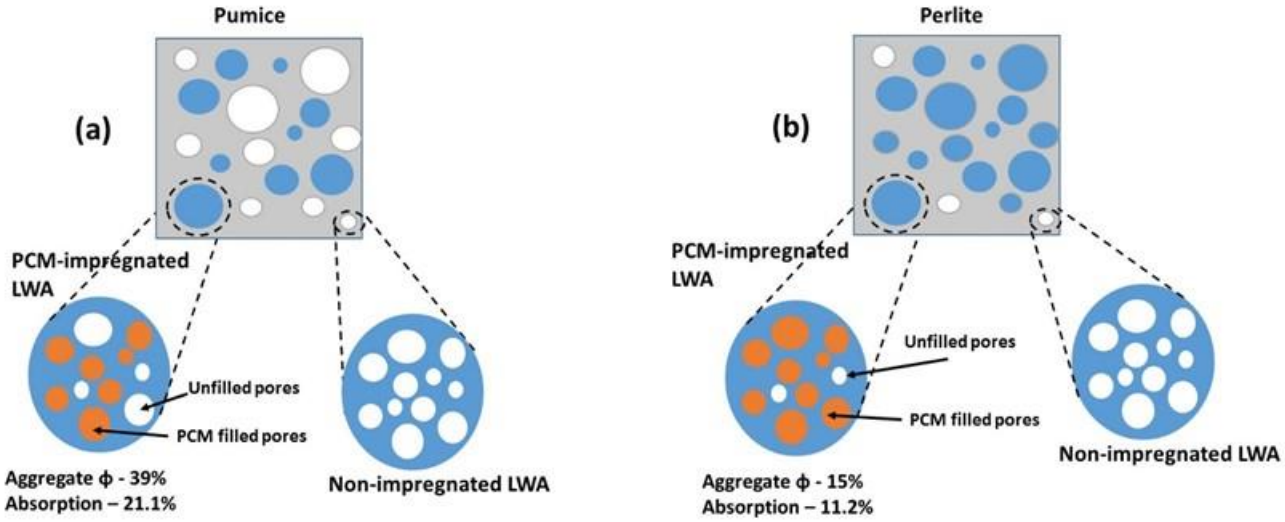

Figure 3: Illustration of the methodology to obtain 5% of PCM in the mortar with: (a) Pumice LWA, and (b) Perlite LWA. Relative amounts of filled and non-filled LWAs in both the cases as well as the saturation levels of LWAs are shown.

Table 1: Mixture proportions (volumetric) used in this study

Mixture	OPC (%)	LWA (%)	CS (%)	PCM (%)
OPC Paste	100	-	-	-
Plain Mortar	50	-	50	-
Mortar with LWAs (PU0, PE0, ES0, ESC0)	50	50	-	-
Mortar with PCM-impregnated LWAs (PU5, PE5, ES5, ESC5)	50	45	-	5

2.4 Test Methods

The porosities of the different LWAs prior to impregnation were determined using mercury intrusion porosimetry (MIP) on oven dried samples. The dried LWA samples were tested in a mercury porosimeter that is capable of exerting a maximum pressure of 414 MPa. The relationship between pore diameter and intrusion pressure was determined using the Washburn equation, based on the assumption that the pores are cylindrical in shape [21]. The contact angle and surface tension values used in this study were 117^{o} and 0.485 N/m respectively [22].

The compressive strengths of mortars containing both the non-impregnated and PCM-impregnated LWAs were determined in accordance with ASTM C109 on 50 mm cubes at different ages.

The thermal properties (e.g. onset, peak, and phase change temperatures, enthalpy, and specific heat capacity) of the LWAs and PCM-impregnated LWAs were determined using a differential scanning calorimeter (DSC) in accordance with ASTM E1269-11. Four replicates for each specimen type were tested using aluminum pans, where samples were uniformly distributed across the bottom of the pan prior to each run. The thermal program used for analysis included a temperature sweep where the sample was heated from -10°C-to-50°C followed by a ramp down cooling to -10°C in an inert nitrogen environment. A rate of temperature change (i.e., heating and cooling) of 5°C/min was used. Prior to testing of the LWA samples, heat flow calibration was performed using a sapphire standard reference. Equation 1 was used to determine the specific heat capacity (C_p), in J/(g.K) of the LWA prior to PCM impregnation.

$$C_p(s) = C_p(st) \cdot \frac{D_s \cdot W_{st}}{D_{st} \cdot W_s} \quad (1)$$

Here $C_p(st)$ is the specific heat capacity of the sapphire standard in J/(g.K), W_s is the mass of the specimen (mg), W_{st} is the mass of the sapphire standard (mg), D_s is the vertical displacement between the heat flow curves of the specimen holder (mW) and the specimen at a given temperature, and D_{st} is the vertical displacement between the heat flow curves of the specimen holder and sapphire standard (mW) at a given temperature.

Thermal conductivity was determined in accordance with ASTM C177-13 using a guarded hot plate apparatus (Figure 4(a)) where measured power is applied to the hot plate in a centralized metered section. The central meter section (Figure 4(b)) is surrounded by thermally isolated guards (a small gap separates the hot plate and guards), thus enabling one-dimensional heat flow. Heat sinks located on the top and bottom of the apparatus remove the heat and provide uniform temperatures at the outer surfaces of the specimen. Two identical (300 x 300 x 12 mm) plate specimens were used to ensure symmetrical heat flow, and averaged to obtain the final thermal conductivity. Specimens for thermal conductivity were tested after 28 days of hydration and allowed to dry for in ambient conditions for 24 hours prior to testing. The duration of testing for each specimen was between 6-10 hours, in order to establish a steady-state temperature gradient over the thickness of the specimen. Thermal conductivity (λ) was determined from the Fourier equation as:

$$\lambda = \frac{qL}{2A(T_h - T_c)} \quad (2)$$

where q is the power input to the central heater, L is the thickness of the specimen, A is the surface area of the central heater, T_h is the temperature of the hot face, and T_c is the temperature of the cold face.

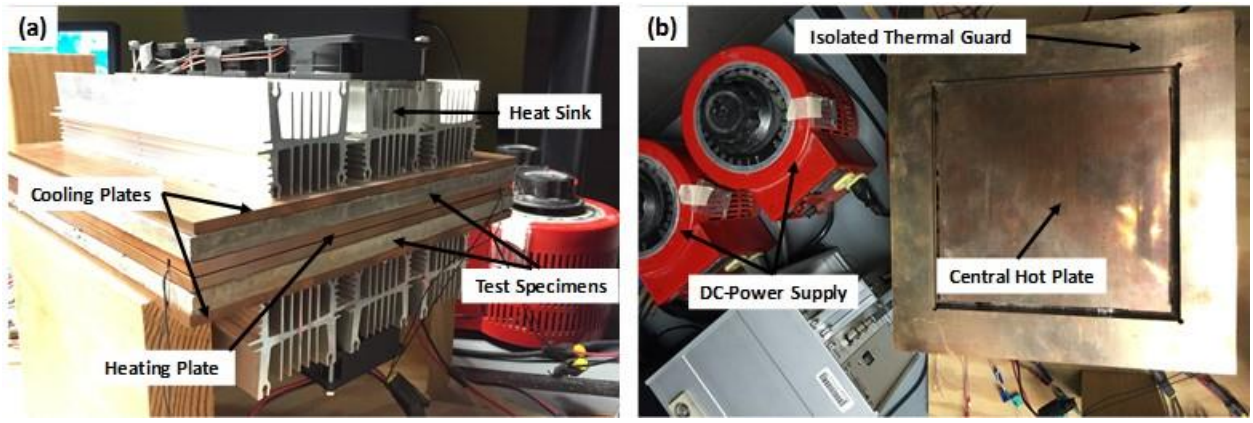

Figure 4: (a) Side profile of the guarded hot plate apparatus and (b) aerial profile of the centralized metered section for determining thermal conductivity.

3. RESULTS AND DISCUSSIONS

3.1. Characteristics of Lightweight Aggregates

Obtaining the appropriate physical properties and pore structure characteristics of LWA that are important in PCM impregnation is critical towards material design of thermally efficient cementitious systems. Figure 5 shows the relationship between pore size and volume of mercury intruded for the LWAs studied. Table 2 shows average specific gravities (oven and saturated surface dry), average pore diameters, porosities, and the PCM absorption capacities after 72 hours of immersion, of the four different LWAs. It is clearly seen that the physical properties of the LWAs are quite different from each other, attributable to the source of the aggregates and their processing. The PCM absorption capacity is an important parameter that dictates the thermal efficiency of the composite. The pumice and expanded shale/clay aggregates show higher PCM absorption capacities than those of perlite and expanded slate. Since the soaking of LWA by PCM was carried out under ambient conditions (i.e., no vacuum), absorption is a function of easily accessible porosity and the sizes of pores. Even though the porosity of expanded shale/clay LWA is about 10% higher than that of the pumice LWA, it has a PCM absorption that is about 5% less than that of pumice. This can be attributed to the average pore diameter of the pumice LWA being 30% greater than that of the expanded shale/clay. Larger pore sizes at comparable porosities ensure larger absorption as can be noticed in the comparison between pumice and expanded slate LWAs in Table 2. For the perlite LWA, the porosity is the lowest but the absorption capacity is comparable to that of expanded

slate LWA because of much larger pore sizes which allow the PCM to absorb into most of the available pore spaces.

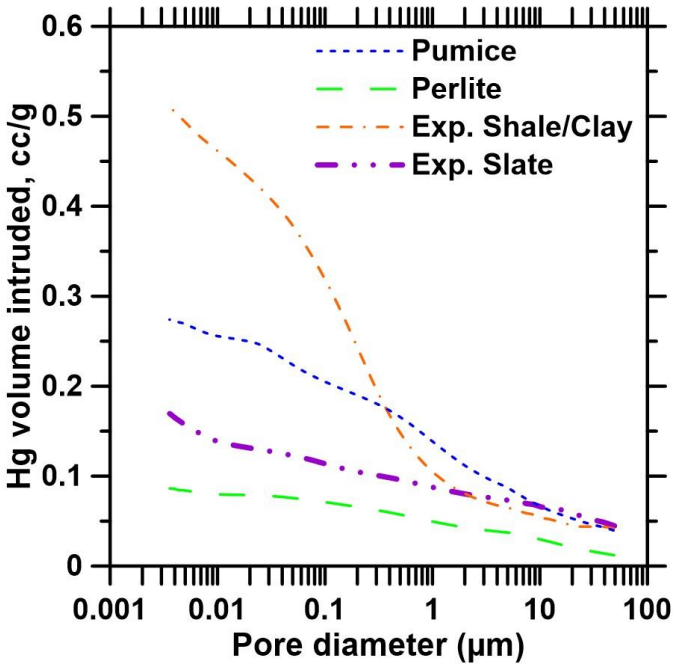

Figure 5: Pore diameter-pore volume relationships curves for the four different LWA types.

Table 2: Physical properties of lightweight aggregates

LWA	S.G. (OD)	S.G. (SSD)	PCM Absorption capacity, % by vol.	Average Pore Diameter (µm)	Porosity
Pumice	1.45	1.75	21.1	516	0.39
Perlite	1.72	1.81	11.2	580	0.15
Exp. Shale/Clay	1.07	1.33	15.7	361	0.53
Exp. Slate	1.77	1.99	10.6	247	0.30

3.2. Compressive Strength of PCM-impregnated LWA Mortars

Previous studies have indicated that the PCMs have the propensity to leak out of the LWA host, and interfere with cement hydration, thereby influencing the mechanical properties of concrete [12,23]. The compressive strength development as a function of curing time for LWA mortars without and with 5% (of the total mortar volume) of PCMs impregnated in the LWAs, are shown in Figures 6(a) and (b) respectively. A comparison of these figures reveal that the compressive strengths remain invariant of both the LWA type and PCM incorporation in the LWAs. These results establish that LWAs can be used as effective

carriers of PCM without adversely influencing the physico-chemical mechanisms that are dominant in strength development. It also shows that the pre-treatment and PCM impregnation methodology described earlier can be adopted effectively without any leakage of PCM from the LWAs into the matrix. In previous studies, when there was potential for such leakage, cement paste coating on the LWAs was found to solve the issue [24,25].

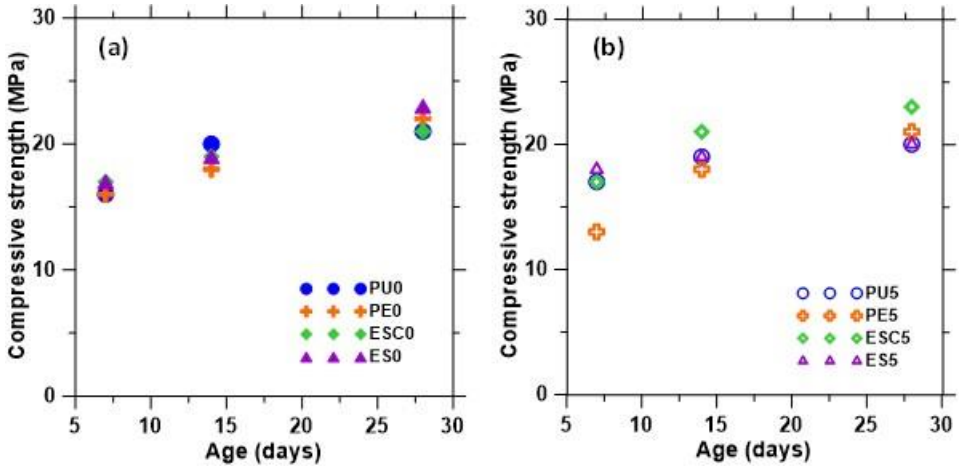

Figure 6: Compressive strengths as a function of time for: (a) plain LWA mortars, and (b) LWA mortars containing 5% PCM by total mortar volume, impregnated in the pores of the LWAs. The standard deviation in compressive strengths ranged between 2 and 3 MPa at early ages and 1 and 2 MPa at later ages.

3.3. Thermal Characterization of LWAs and LWA-PCM Mortars

3.3.1. Enthalpy of fusion (ΔH_f^0)

Figure 7 shows the endothermic heat flow peak for the four different LWAs impregnated with PCM (up to their absorption capacity, Table 2), after 72 hours of absorption. The endothermic peak represents the heat being absorbed by the PCM (latent energy storage), as a result of phase transition. The onset temperature (T_{onset}) corresponding to melting is 17.3 $\pm$0.15°C and the completion temperature ($T_{completion}$) is 27.5 $\pm$0.15°C. The melting point or endothermic peak occurs at 24°C for all the LWA-PCM combinations, which is the intrinsic phase change temperature of the PCM. The difference in heat flow curves between different LWA-PCM combinations is a result of the differences in the PCM absorption capacity of the LWA (Table 2). Unsurprisingly, the degree of PCM absorption, which in turn depends on the pore structure of the LWA, influences the thermal energy storage. The total area under the heat flow curve in the temperature range between the onset and completion of phase transition, which corresponds to the enthalpy of the composite, is shown for all the LWA-PCM combinations in Table 3. The theoretical enthalpy was determined from the amount of PCM (by mass) absorbed in the different LWA types and

the heat storage capacity (heat of fusion) provided by the manufacturer for the chosen PCM, which in this case was 184 J/g. The theoretical and experimentally measured enthalpies for all the combinations are quite similar, with the measured enthalpies being slightly higher. This can be attributed to the likely presence of small amounts of PCM that adhere to the surface of the LWAs even after the draining process. The results presented are the average of three DSC runs for a given sample. The standard deviations ranged from 4%-to-15%.

DSC was also used to determine the specific heat capacity of the pristine LWAs as described earlier. The specific heat capacities of all the LWAs were determined at a temperature of 27.5°C (beyond the PCM phase transition). The measured specific heat capacity, shown in Table 4, ranges between 0.62-to-0.91 J/g-K, and are very similar to those reported for these materials [26–29].

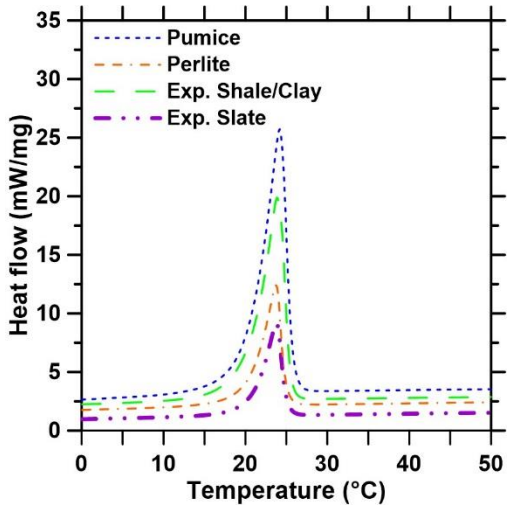

Figure 7: DSC curves of LWAs impregnated with PCM, after 72 hours of absorption.

Table 3: Enthalpy comparison of the LWA-impregnated PCMs

LWA+PCM	Measured Enthalpy (J/g)	Theoretical Enthalpy (J/g)
Pumice	31.66	30.42
Perlite	14.45	11.78
Exp. Shale/Clay	34.26	28.70
Exp. Slate	12.24	11.40

Table 4: Specific heat capacity of the LWAs

LWA	Specific Heat Capacity (J/g-K)
Pumice	0.91
Perlite	0.62
Exp. Shale/Clay	0.68
Exp. Slate	0.88

3.3.2. Thermal conductivity of LWA mortars

The thermal conductivity of all the mortars evaluated here are shown in Figure 5. The thermal conductivities have been determined in the saturated condition. In other words, the accessible pores in the LWA that contribute to its absorption capacity (Table 2) are filled with water or water and PCM. The thermal conductivity is the highest for the conventional OPC mortar because of the higher thermal conductivity of the dense quartz particles [30,31]. The reduction in thermal conductivity when regular sand is replaced by lightweight aggregates (irrespective of the LWA type) can be easily noted from this figure. The added advantage of reducing the structural self-weight, and the capability to provision the non-PCM impregnated LWAs with water for internal curing, provides an array of benefits for this methodology. PCM impregnated LWA mortars generally show thermal conductivities that are about 10%-20% lower than the regular LWA (water-saturated) mortars, at a total PCM content of 5% by volume in the mortars. This reduction in thermal conductivity can be attributed to the lower thermal conductivity of the PCM (0.15 W/m-K) as compared to that of water (0.6 W/m-K). In addition, the absorption capacity of the aggregates also influences the thermal conductivity since the pores that are not accessible to water and/or PCM are filled with air that has a much lower thermal conductivity than any of the other constituents. Densification of the interface layer in LWA mortars [32] influences heat transfer and could result in diminishing some of the effects of porosity-induced thermal conductivity reduction. The porosity and surface characteristics of LWAs are thus also important. The thermal conductivity experiments show that, in addition to the latent heat capacity of PCMs that help reduce energy consumption when used in building envelopes, the enhanced insulation properties of LWA concrete containing PCMs also will be beneficial in energy efficient construction. The methodology can be easily implemented in concrete masonry units and precast concrete wall and roof panels.

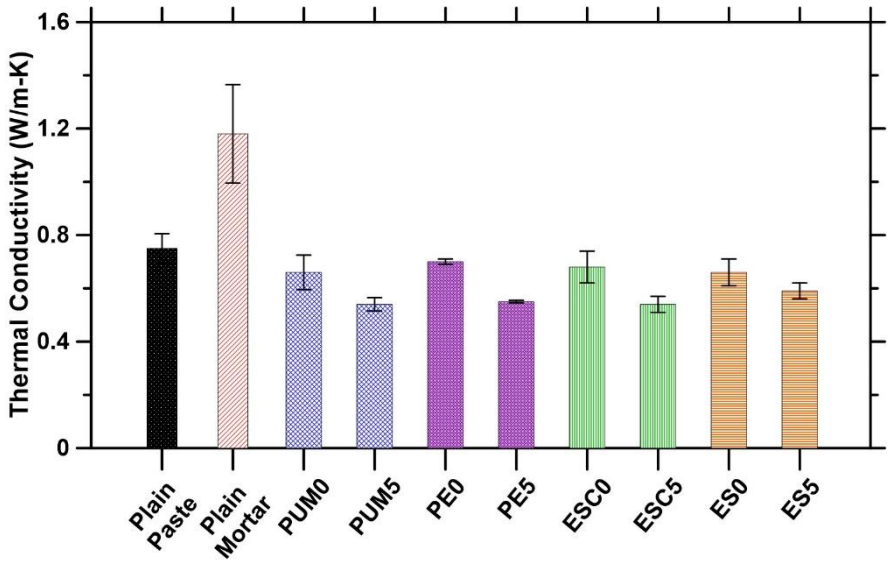

Figure 8: Thermal conductivity determined after 28 days of hydration for the paste and mortars. The first data is for OPC paste, and the rest are for mortars where the paste volume fraction is 0.50.

3.4. Application of Homogenization Models for Thermal Conductivity Prediction of LWA-PCM Composite Mortars

As noted earlier in this paper, LWAs, when incorporated in cementitious materials, are random multi-phase media consisting of the solid phase, and the distributed pore phases that can contain a combination of air, water and/or PCM. Thus, in contrast to general multi-phase media which consists of one continuous matrix and multiple inclusion types, the LWA mortars consist of an inclusion phase which by itself is bi- or tri-phasic, as shown in Figure 9. Accurately predicting the engineering behavior (mechanical, electrical, thermal etc.) of such multi-phase materials is a challenging task. For two-phase composites (matrix and one type of inclusion) with an ordered microstructure, exact models exist. When the microstructure is random, bounds on effective properties are usually adopted [33,34]. Effective medium theories (EMT), such as Bruggeman's unsymmetrical EMT and self-consistent symmetrical EMT [35], and generalized effective medium theories [36,37] for composite properties including conductivity have been proposed and validated. When phase-geometry information is available along with the volume fraction, then much narrower bounds can be attained. For example, mean field homogenization models use the aspect ratio and orientation of the inclusion phase to provide accurate property descriptors [38,39]. In this paper, attempt is made to predict the effective thermal conductivity of cementitious mortars containing LWAs impregnated with PCM using a simple analytical model and a simplified mean field homogenization model. Accurate prediction of thermal properties helps develop mixture proportions for such composite mortars, including the amount and type of LWA and PCM needed for desired thermal performance. However, it

needs to be noted that these models cannot take into account clustering, percolation and size effects, which can be accomplished only using detailed numerical modeling schemes.

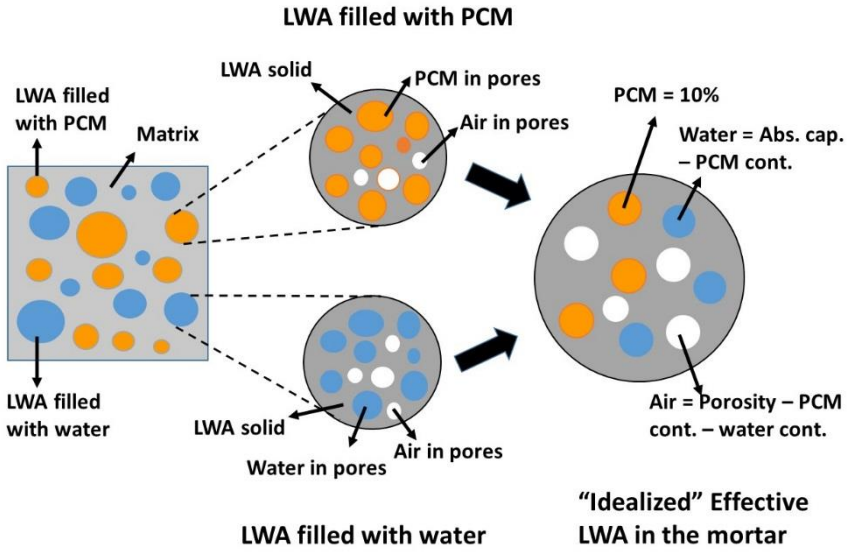

Figure 9: Idealized LWA for effective property determination. Some LWAs have PCM while some others have water to ensure desired PCM levels in the mortars. An "idealized" LWA is also shown, that is representative of the LWA phase.

Homogenization is executed here for a two-phase composite (cement paste and LWA). However, LWA being a multi-phase heterogeneous composite in its own right (containing a solid phase, and pores containing water, air, or PCM), its effective thermal property is determined by a separate homogenization process. Accurate determination of the volume fractions of the appropriate phases, the intrinsic thermal conductivity of solid phase in LWAs (considering that the thermal conductivities of water, air, and PCM are known), and the effective thermal conductivity of the LWA, are needed for the property prediction of the mortar. It is emphasized that the effective property of LWA as stated here is not for an individual LWA particle, but a representative one for the entire LWAs present in a certain mortar. Realistically, some LWAs in the mortar contain water and air voids, while some others contain PCM and air voids. The "idealized" LWA particle combines both these types as shown in Figure 9.

3.4.1. Volume Fractions of component phases

Since all the mortars were proportioned for 5% of PCM by total volume, and the mortars contain 50% by volume of LWA, the volume of PCM as a fraction of total LWA volume is 10%. The remaining pore volume of the LWAs is filled with water and air. The amount of water filled pores is determined by subtracting the PCM volume from the LWA absorption capacity, and the remaining fraction of porosity is considered as

air voids. The volume fraction of water filled pores in the LWA mortars without PCM is the same as its absorption capacity. Table 5 presents the individual phase volume fractions in the different LWAs.

Table 5: Fractions of solid, water, PCM, and air in the LWAs in the PCM-impregnated mortars. The water comes from the saturated, non-PCM impregnated LWAs added to ensure that the total PCM volume fraction is 5%.

LWA	Porosity	Solid fraction	Absorption capacity	PCM content	Water content	Air void content
Pumice	0.39	0.61	0.211	0.1	0.111	0.179
Perlite	0.15	0.85	0.112	0.1	0.012	0.038
Exp. Slate	0.30	0.7	0.106	0.1	0.006	0.194
Exp. Shale/Clay	0.53	0.47	0.157	0.1	0.057	0.373

3.4.2. Intrinsic thermal properties of component phases

Having known the volume fractions of the phases, it is then necessary to obtain the intrinsic thermal properties of the individual phases within the LWA particle to determine the effective thermal properties of LWAs. The thermal conductivities of water, air, and PCM (0.6, 0.15, and 0.025 W/m-K respectively) are known [40,41]. The thermal conductivity of the solid phase of the different LWAs was obtained in this study through an inverse analysis procedure using the Mori-Tanaka approach [42,43,38] as detailed below.

Mori-Tanaka homogenization method has been used for the determination of effective properties of cement-based materials [44–47]. It approximates the interaction between the different phases by considering that each inclusion is embedded, in turn, in an infinitely extended homogeneous reference medium (matrix) that is subjected to a temperature gradient. In other words, each inclusion behaves like an isolated inclusion in the matrix experiencing the average temperature gradient in the matrix as the far-field gradient. The effective thermal conductivity based on Mori-Tanaka model is given as [43]:

$$\lambda^{(c)} = \lambda^{(m)} + v^{(i)}(\lambda^{(i)} - \lambda^{(m)})\overline{A}^{i}_{MT} \tag{3}$$

Here, $\lambda^{(c)}$ is the effective composite thermal conductivity; $\lambda^{(m)}$ is the thermal conductivity of matrix; $\lambda^{(i)}$ is the thermal conductivity of inclusion, $v^{(i)}$ is the inclusion volume fraction and $\overline{A}^{i}_{MT}$ is the Mori-Tanaka gradient concentration tensor of the inclusion, given as [43]:

$$\overline{A}^{i}_{MT} = \overline{A}^{i}_{d}(v^{(m)}I + v^{(i)}\overline{A}^{i}_{d})^{-1} \tag{4}$$

Here, $v^{(m)}$ is the matrix volume fraction, i.e., $v^{(m)} = 1 - v^{(i)}$, I denotes the identity tensor and $\overline{A}_d^i$ is the gradient concentration tensor of dilute inclusions with perfect interfaces, given as [43]:

$$\overline{A}_d^i = [I - SR^{(m)}(\lambda^{(i)} - \lambda^{(m)})]^{-1} \tag{5}$$

Where $R^{(m)}$ is the resistivity tensor, given as $R^{(m)} = (\lambda^{(m)})^{-1}$ and S is the Eshelby tensor [43,48]. For multiple spherical inclusions of isotropic thermal conductivity embedded in a matrix, Equation 3 reduces to a scalar expression as [38,49]:

$$\lambda^c = \frac{v^m \lambda^m + \sum_{i=1}^{N} v^i \lambda^i \frac{3\lambda^m}{2\lambda^m + \lambda^i}}{v^m + \sum_{i=1}^{N} v^i \frac{3\lambda^m}{2\lambda^m + \lambda^i}} \tag{6}$$

The experimentally measured thermal conductivities of the plain LWA mortars (without PCM) were used in a two-step inverse analysis procedure employing the Mori-Tanaka method to obtain the thermal conductivity of solid phase in different LWAs. The steps are schematically shown in Figure 10. In the first step, the experimental thermal conductivity of the different LWA mortars and the known thermal conductivity of the cement paste phase (see Figure 8) are used to back-calculate the thermal conductivity of the different LWAs. The second step calculates the thermal conductivity of solid phase of the LWA from the homogenized thermal conductivity of LWA obtained from step-I and the already known thermal conductivities of air and water. The LWA is considered as a three-phase composite here. The solid phase thermal conductivities obtained for pumice, perlite, expanded slate, and expanded shale/clay are 0.8, 0.59, 0.82 and 1.1 W/m-K respectively, reflecting the differences in the mineralogy of these LWAs. The values of thermal conductivity of the solid phase of the LWAs thus obtained from inverse analysis are used in further simulations to determine effective thermal conductivity of PCM-impregnated LWA mortars.

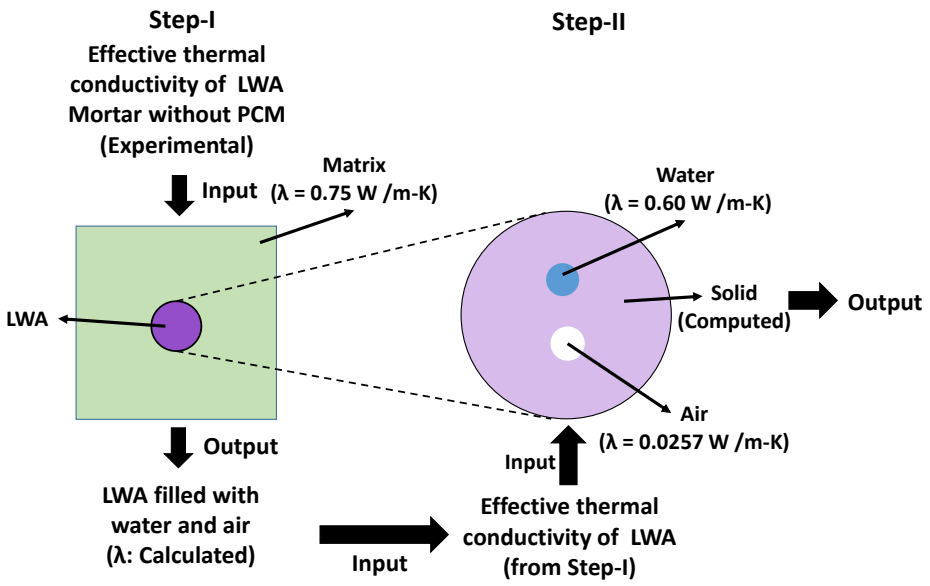

Figure 10: Inverse analysis procedure for the determination of thermal conductivity of the solid phase of LWAs.

3.4.3. Predicting effective thermal conductivity of PCM-impregnated LWA mortars

In this section, analytical and mean-field homogenization models are used to predict the effective thermal conductivities of PCM-impregnated LWA mortars from those of its phases and their volume fractions. Among the several analytical models available, Maxwell-Garnett model is used here since it has been used in the past to predict the thermal conductivity of multiphase particulate composite materials [50,51]. The homogenized thermal conductivity λ^c can be obtained from the thermal conductivities of the matrix (λ^m) and the inclusion (λ^i) phases as:

$$\frac{\lambda^c - \lambda^m}{\lambda^c + 2\lambda^m} = \sum_{i=1}^{N} v^i \left[\frac{\lambda^i - \lambda^m}{\lambda^i + 2\lambda^m} \right] \tag{7}$$

In this equation, v^i the volume fraction of inclusion i and N is the number of inclusion phases.

The simplified mean-field homogenization scheme employs the Mori-Tanaka method [42,43,38]. Two different approaches are implemented as explained below. First, a two-step homogenization process, both involving the Mori-Tanaka scheme, is implemented as shown in Figure 11. In the first step, the water-filled voids, PCM-filled voids and the air voids are homogenized into the solid LWA matrix to obtain the homogenized thermal conductivity of LWA. The second step homogenizes the thermal conductivity of LWA (determined in Step-I) with that of the hardened cement paste matrix to determine the effective thermal conductivity of the PCM-impregnated LWA mortar.

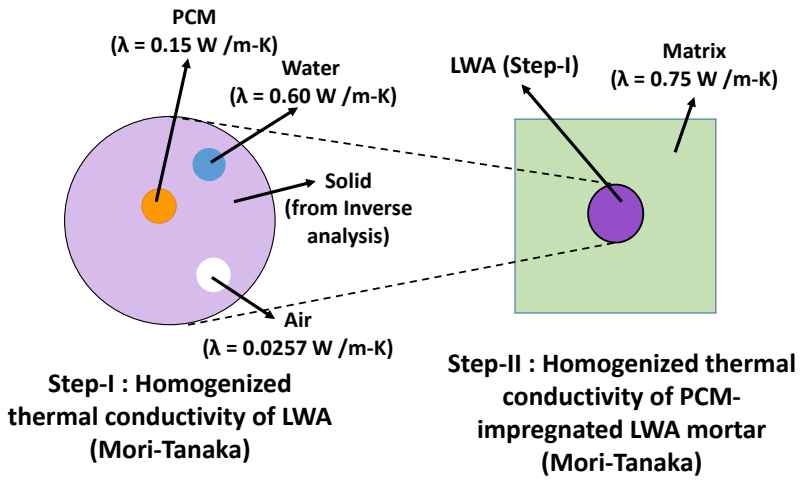

Figure 11: Two-step Mori-Tanaka homogenization scheme for determination of thermal conductivity of PCM-impregnated LWA mortars.

The homogenization method described above relies on the knowledge of the microstructural arrangement in the composite, i.e, the LWA phase is dispersed in the matrix phase. Note that all the three phases in the representative LWA is considered in a single homogenization step. In cases where the microstructural phase arrangement is not a priori known, a sequential homogenization process has to be employed. This approach homogenizes a two-phase media at any given step, and uses the homogenized results in the following step. The order of homogenization relies less on the microstructural arrangement, and is dictated by the property contrast between the phases. Figure 12 depicts the stages in the four-stage homogenization approach, also involving the Mori-Tanaka method. The four-stage homogenization procedure includes the following steps: (i) the first stage of homogenization considers the solid phase of LWAs as the matrix and the water filled pores as inclusions; (ii) the homogenized thermal conductivity obtained from step-I is then input as the matrix for the second stage with the PCM filled pores as inclusions, (iii) in the third step, the resultant of the second stage serves as the matrix to which the air voids are added as inclusions to obtain the effective thermal conductivity of LWA inclusions; (iv) the last step homogenizes the LWAs into the matrix of hardened cement paste to obtain the effective thermal conductivity of PCM-impregnated LWA mortars. This order of homogenization ensures minimization of the effects of thermal conductivity contrast of different phases on the predicted effective property.

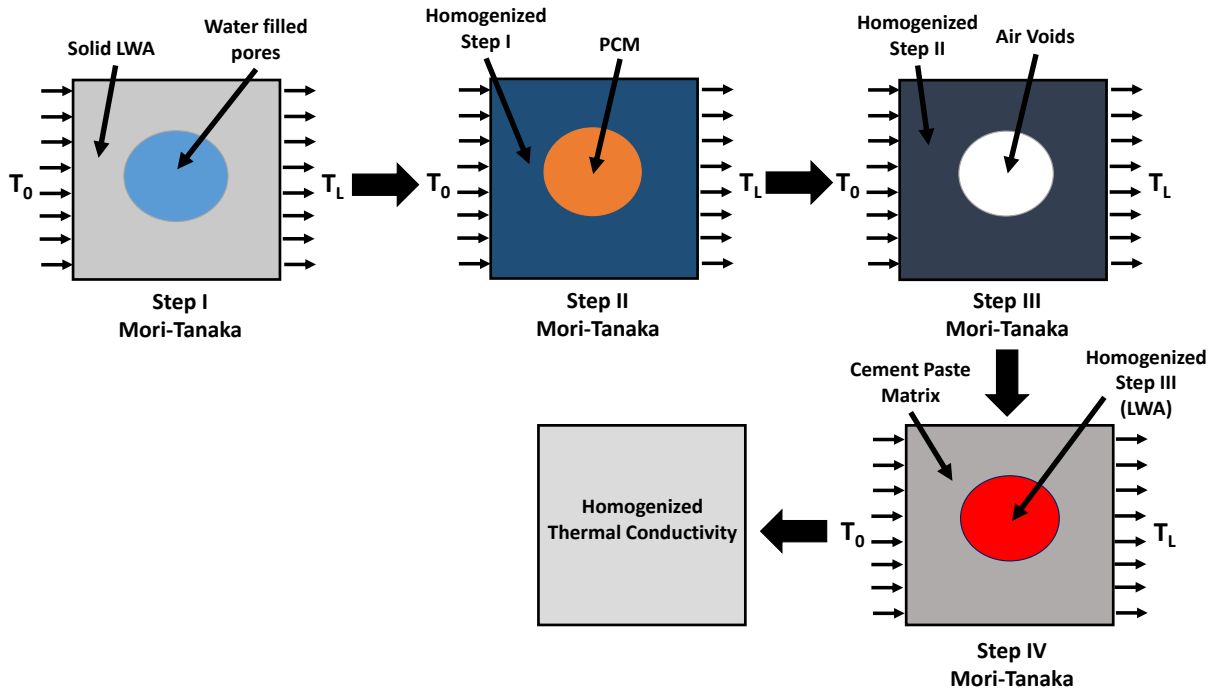

Figure 12: Four-step Mori-Tanaka homogenization scheme for thermal conductivity determination of mortars with PCM-impregnated LWAs.

The effective thermal conductivities of the PCM-impregnated LWA mortars predicted using the Maxwell-Garnett and Mori-Tanaka schemes are shown in Figure 13 (a) along with the corresponding experimental values. It is immediately evident from this figure that the two-step Mori-Tanaka approach results in the closest predictions of thermal conductivity. The differences between the experimental and predicted results range from 7% to 13%, with the largest difference demonstrated for the system that has the highest amount of air voids (expanded shale/clay; Table 5) and the least difference when the volume of air voids are the least (perlite). The thermal conductivity contrast between air voids and the other constituent phases is the largest (one-to-two orders of magnitude), and hence higher volume fractions of air voids result in increased divergence of the predictions from experimental results. Presence of phases with high property contrasts limits accurate prediction of effective properties as reported in [52–54] .

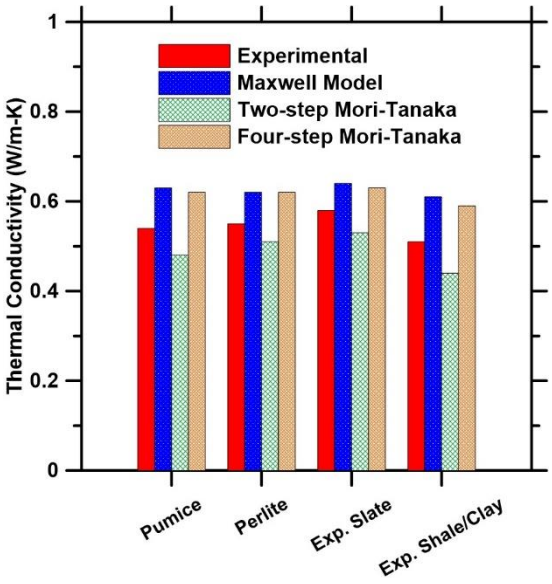

Figure 13: Experimental and predicted thermal conductivity values of PCM-impregnated LWA mortars.

Figure 14(a) shows the average (of all the four LWA mortars) difference between the experimental thermal conductivities and those predicted using the three analytical schemes presented in this paper. It can be seen that the two-step Mori-Tanaka method, that considers the microstructural arrangement (and therefore appropriate inter-phase interactions) is the most reliable among the methods chosen. When property contrast alone is considered as is the case for the four-step method, the predictive efficiency drops. However, both these approaches are more efficient than the Maxwell-Garnett method.

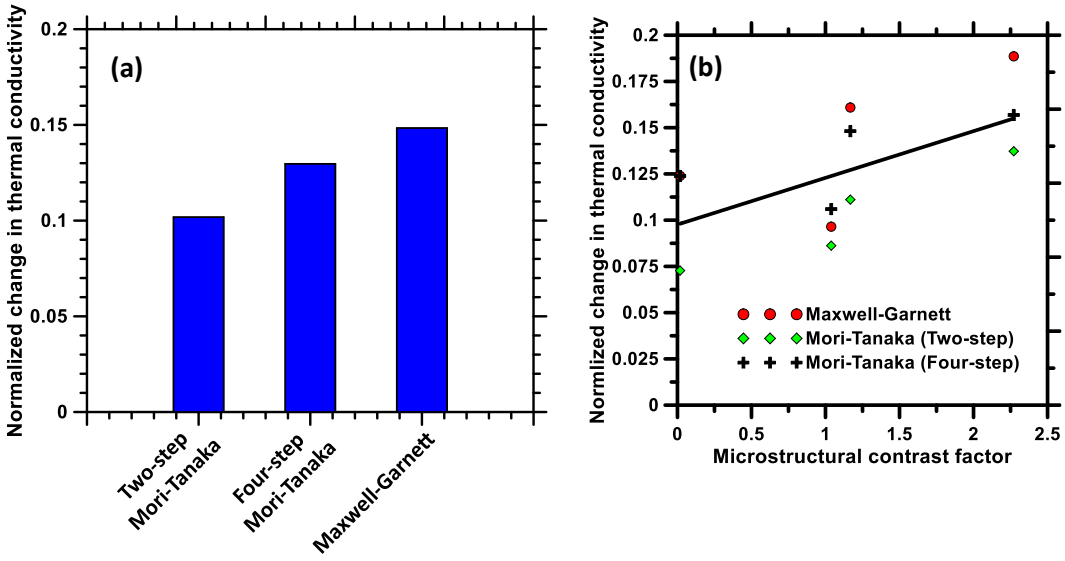

Figure 14: (a) Average deviations between the experimental thermal conductivities and those predicted by the three modeling schemes, and (b) predictive efficiency as a function of the microstructural contrast factor.

To quantify the influence of the microstructural phases and contrasts in their thermal conductivities on the predicted composite, a microstructural contrast factor (ζ) is defined as shown below:

$$\zeta = \left(\frac{\lambda_s}{v_s} - \frac{\lambda_{air}}{v_{air}} \right) \tag{8}$$

Here, λ_s is the thermal conductivity of solid phase of the LWA, λ_{air} is the thermal conductivity of air, v_s is the volume fraction of solid phase in LWAs and v_{air} is the volume fraction of air voids in LWAs. This factor accounts for both the thermal conductivities as well as the volume fractions of the phases with the highest property contrast. Figure 14(b) shows the relationship between the contrast factor and the normalized change in thermal conductivity ($\Delta\lambda/\lambda_{exp}$), where $\Delta\lambda$ is the absolute difference between the experimental and predicted thermal conductivities and λ_{exp} is the experimental thermal conductivity. A smaller value of $\Delta\lambda/\lambda_{exp}$ indicates better predictive efficiency of the model. It is shown that an increase in ζ results in lower predictive efficiencies, thereby quantifying the influence of volume fractions and properties of the contrasting phases on the predictive capabilities of analytical models.

4. CONCLUSIONS

A comprehensive study on the influence of LWA characteristics on PCM impregnation efficiencies, and the resulting thermal properties of the mortars has been reported. Four different LWAs of different

mineralogy and pore structure features were used. The mixtures were designed to ensure 5% of PCM by volume of the mortar. This necessitated a proportioning procedure that included both PCM–impregnated and non-impregnated LWAs, depending on their porosity and absorption capacity. The LWA mortars containing 5% of PCM showed thermal conductivities that are 10% or more lower as compared to those of the plain LWA mortars, which can be attributed to the much lower thermal conductivity of PCM as compared to water. In addition to enhancing the insulating capacity of the composite mortars used as building elements, the incorporation of PCMs also compensates to some degree for the loss of thermal inertia in lightweight systems because of their heat storage and release capacity that reduces temperature fluctuations in the building.

Maxwell-Garnett effective medium, and Mori-Tanaka mean-field homogenization models were used to predict the thermal conductivity of LWA-PCM mortars. The thermal conductivities of the solid phase of the LWAs were determined using an inverse analysis procedure. The application of Mori-Tanaka method included: (i) a two-step process based on known microstructural arrangement of the composite where the homogenized LWA was incorporated into a cement paste matrix, or (ii) a four-step process where each of the microstructural constituents (solid, pore, air, and water phases of LWA and the cement paste) were sequentially homogenized based on the thermal conductivity contrast between the phases. The two-step Mori-Tanaka approach resulted in the thermal conductivity predictions being closest to the experimental values, and the Maxwell-Garnett predictions diverged the most. The understanding that the relative volume fractions of phases with the largest property contrasts (in this case, the solid phase of LWA and air), and the magnitude of these property contrasts impact the accuracy of analytical predictive schemes led to the development of a microstructural contrast factor. This factor was found to be very well related to the normalized difference in the experimental and predictive thermal conductivities.

5. ACKNOWLEDGEMENTS

The authors gratefully acknowledge partial supports from the National Science Foundation (CMMI: 1130028) and an Infravation ERA-NET Plus grant (31109806.0001) of the European Commission towards this study. MA acknowledges a Dean's Fellowship from the Ira A. Fulton Schools of Engineering at Arizona State University (ASU). NK acknowledges support from The Scientific and Technological Research Council of Turkey (TUBITAK). Entropy Solutions is acknowledged for the supply of PCMs while Stalite, Hess Pumice Products, Trinity Lightweight are acknowledged for supplying the lightweight aggregates. The contents of this paper reflect the views of the authors who are responsible for the facts and accuracy of the data presented herein, and do not necessarily reflect the views and policies of the funding agency, nor do the contents constitute a standard, specification, or a regulation. We gratefully acknowledge the use of

facilities within the Structural Engineering Laboratory and the Laboratory for the Science of Sustainable Infrastructural Materials (LS-SIM) at Arizona State University.

6. REFERENCES

[1] B. Zalba, J.M. Marín, L.F. Cabeza, H. Mehling, Review on thermal energy storage with phase change: materials, heat transfer analysis and applications, Appl. Therm. Eng. 23 (2003) 251–283. doi:10.1016/S1359-4311(02)00192-8.

[2] A. Sharma, V.V. Tyagi, C.R. Chen, D. Buddhi, Review on thermal energy storage with phase change materials and applications, Renew. Sustain. Energy Rev. 13 (2009) 318–345. doi:10.1016/j.rser.2007.10.005.

[3] K. Pielichowska, K. Pielichowski, Phase change materials for thermal energy storage, Prog. Mater. Sci. 65 (2014) 67–123. doi:10.1016/j.pmatsci.2014.03.005.

[4] M.K. Rathod, J. Banerjee, Thermal stability of phase change materials used in latent heat energy storage systems: A review, Renew. Sustain. Energy Rev. 18 (2013) 246–258. doi:10.1016/j.rser.2012.10.022.

[5] L. Cao, D. Su, Y. Tang, G. Fang, F. Tang, Properties evaluation and applications of thermal energystorage materials in buildings, Renew. Sustain. Energy Rev. 48 (2015) 500–522. doi:10.1016/j.rser.2015.04.041.

[6] S.A. Memon, Phase change materials integrated in building walls: A state of the art review, Renew. Sustain. Energy Rev. 31 (2014) 870–906. doi:10.1016/j.rser.2013.12.042.

[7] L. Hembade, S.D. Rajan, N. Neithalath, A finite-element based framework for understanding the energy performance of concrete structural elements containing phase change materials, ASCE J. Energy Eng. Accepted (n.d.).

[8] F. Kuznik, D. David, K. Johannes, J.-J. Roux, A review on phase change materials integrated in building walls, Renew. Sustain. Energy Rev. 15 (2011) 379–391. doi:10.1016/j.rser.2010.08.019.

[9] V.V. Tyagi, S.C. Kaushik, S.K. Tyagi, T. Akiyama, Development of phase change materials based microencapsulated technology for buildings: A review, Renew. Sustain. Energy Rev. 15 (2011) 1373–1391. doi:10.1016/j.rser.2010.10.006.

[10] M. Delgado, A. Lázaro, J. Mazo, B. Zalba, Review on phase change material emulsions and microencapsulated phase change material slurries: Materials, heat transfer studies and applications, Renew. Sustain. Energy Rev. 16 (2012) 253–273. doi:10.1016/j.rser.2011.07.152.

[11] A. Joulin, L. Zalewski, S. Lassue, H. Naji, Experimental investigation of thermal characteristics of a mortar with or without a micro-encapsulated phase change material, Appl. Therm. Eng. 66 (2014) 171–180. doi:10.1016/j.applthermaleng.2014.01.027.

[12] S.A. Memon, H.Z. Cui, H. Zhang, F. Xing, Utilization of macro encapsulated phase change materials for the development of thermal energy storage and structural lightweight aggregate concrete, Appl. Energy. 139 (2015) 43–55. doi:10.1016/j.apenergy.2014.11.022.

[13] A.R. Sakulich, D.P. Bentz, Incorporation of phase change materials in cementitious systems via fine lightweight aggregate, Constr. Build. Mater. 35 (2012) 483–490. doi:10.1016/j.conbuildmat.2012.04.042.

[14] N.P. Sharifi, A. Sakulich, Application of phase change materials to improve the thermal performance of cementitious material, Energy Build. 103 (2015) 83–95. doi:10.1016/j.enbuild.2015.06.040.

[15] M.C.S. Nepomuceno, P.D. Silva, Experimental evaluation of cement mortars with phase change material incorporated via lightweight expanded clay aggregate, Constr. Build. Mater. 63 (2014) 89–96. doi:10.1016/j.conbuildmat.2014.04.027.

[16] D.P. Bentz, R. Turpin, Potential applications of phase change materials in concrete technology, Cem. Concr. Compos. 29 (2007) 527–532. doi:10.1016/j.cemconcomp.2007.04.007.
[17] F. Fernandes, S. Manari, M. Aguayo, K. Santos, T. Oey, Z. Wei, G. Falzone, N. Neithalath, G. Sant, On the Feasibility of Using Phase Change Materials (PCMs) to Mitigate Thermal Cracking in Cementitious Materials, Cem. Concr. Compos. (n.d.). doi:10.1016/j.cemconcomp.2014.03.003.
[18] D. Zhang, Z. Li, J. Zhou, K. Wu, Development of thermal energy storage concrete, Cem. Concr. Res. 34 (2004) 927–934. doi:10.1016/j.cemconres.2003.10.022.
[19] D. Zhang, S. Tian, D. Xiao, Experimental study on the phase change behavior of phase change material confined in pores, Sol. Energy. 81 (2007) 653–660. doi:10.1016/j.solener.2006.08.010.
[20] T. Nomura, N. Okinaka, T. Akiyama, Impregnation of porous material with phase change material for thermal energy storage, Mater. Chem. Phys. 115 (2009) 846–850. doi:10.1016/j.matchemphys.2009.02.045.
[21] E.W. Washburn, Note on a Method of Determining the Distribution of Pore Sizes in a Porous Material, Proc. Natl. Acad. Sci. U. S. A. 7 (1921) 115–116.
[22] A.A. Liabastre, C. Orr, An evaluation of pore structure by mercury penetration, J. Colloid Interface Sci. 64 (1978) 1–18. doi:10.1016/0021-9797(78)90329-6.
[23] M. Hunger, A.G. Entrop, I. Mandilaras, H.J.H. Brouwers, M. Founti, The behavior of self-compacting concrete containing micro-encapsulated Phase Change Materials, Cem. Concr. Compos. 31 (2009) 731–743. doi:10.1016/j.cemconcomp.2009.08.002.
[24] M. Kheradmand, J. Castro-Gomes, M. Azenha, P.D. Silva, J.L.B. de Aguiar, S.E. Zoorob, Assessing the feasibility of impregnating phase change materials in lightweight aggregate for development of thermal energy storage systems, Constr. Build. Mater. 89 (2015) 48–59. doi:10.1016/j.conbuildmat.2015.04.031.
[25] X. Li, J.G. Sanjayan, J.L. Wilson, Fabrication and stability of form-stable diatomite/paraffin phase change material composites, Energy Build. 76 (2014) 284–294. doi:10.1016/j.enbuild.2014.02.082.
[26] D.J. Sailor, D. Hutchinson, L. Bokovoy, Thermal property measurements for ecoroof soils common in the western U.S., Energy Build. 40 (2008) 1246–1251. doi:10.1016/j.enbuild.2007.11.004.
[27] D.J. Sailor, M. Hagos, An updated and expanded set of thermal property data for green roof growing media, Energy Build. 43 (2011) 2298–2303. doi:10.1016/j.enbuild.2011.05.014.
[28] S. Andersson, L. Dzhavadov, Thermal conductivity and heat capacity of amorphous SiO 2 : pressure and volume dependence, J. Phys. Condens. Matter. 4 (1992) 6209. doi:10.1088/0953-8984/4/29/005.
[29] M. Zukowski, G. Haese, Experimental and numerical investigation of a hollow brick filled with perlite insulation, Energy Build. 42 (2010) 1402–1408. doi:10.1016/j.enbuild.2010.03.009.
[30] K.-H. Kim, S.-E. Jeon, J.-K. Kim, S. Yang, An experimental study on thermal conductivity of concrete, Cem. Concr. Res. 33 (2003) 363–371. doi:10.1016/S0008-8846(02)00965-1.
[31] W.F. Waite, B.J. deMartin, S.H. Kirby, J. Pinkston, C.D. Ruppel, Thermal Conductivity Measurements in Porous Mixtures of Methane Hydrate and Quartz Sand, Geophys. Res. Lett. 29 (2002) 2229. doi:10.1029/2002GL015988.
[32] H. Uysal, R. Demirboğa, R. Şahin, R. Gül, The effects of different cement dosages, slumps, and pumice aggregate ratios on the thermal conductivity and density of concrete, Cem. Concr. Res. 34 (2004) 845–848. doi:10.1016/j.cemconres.2003.09.018.
[33] Z. Hashin, S. Shtrikman, A Variational Approach to the Theory of the Effective Magnetic Permeability of Multiphase Materials, J. Appl. Phys. 33 (1962) 3125–3131. doi:10.1063/1.1728579.
[34] G.W. Milton, Concerning bounds on the transport and mechanical properties of multicomponent composite materials, Appl. Phys. A. 26 (1981) 125–130. doi:10.1007/BF00616659.

[35] A.M. Jayannavar, N. Kumar, Generalization of Bruggeman's unsymmetrical effective-medium theory to a three-component composite, Phys. Rev. B. 44 (1991) 12014–12015. doi:10.1103/PhysRevB.44.12014.
[36] D.S. McLachlan, Measurement and analysis of a model dual-conductivity medium using a generalised effective-medium theory, J. Phys. C Solid State Phys. 21 (1988) 1521. doi:10.1088/0022-3719/21/8/025.
[37] W.-Z. Cai, S.-T. Tu, J.-M. Gong, A Physically Based Percolation Model of the Effective Electrical Conductivity of Particle Filled Composites, J. Compos. Mater. 40 (2006) 2131–2142. doi:10.1177/0021998306062312.
[38] J. Stránský, J. Vorel, J. Zeman, M. Šejnoha, Mori-Tanaka Based Estimates of Effective Thermal Conductivity of Various Engineering Materials, Micromachines. 2 (2011) 129–149. doi:10.3390/mi2020129.
[39] O. Pierard, C. Friebel, I. Doghri, Mean-field homogenization of multi-phase thermo-elastic composites: a general framework and its validation, Compos. Sci. Technol. 64 (2004) 1587–1603. doi:10.1016/j.compscitech.2003.11.009.
[40] K. Kadoya, M.J. Matsunaga, A. Nagashima, Viscosity and Thermal Conductivity of Dry Air in the Gaseous Phase, J. Phys. Chem. Ref. Data. 14 (1985) 947–970.
[41] M.L.V. Ramires, C.A.N. de Castro, Y. Nagasaka, A. Nagashima, M.J. Assael, W.A. Wakeham, Standard Reference Data for the Thermal Conductivity of Water, J. Phys. Chem. Ref. Data. 24 (1995) 1377–1381. doi:10.1063/1.555963.
[42] T. Mori, K. Tanaka, Average stress in matrix and average elastic energy of materials with misfitting inclusions, Acta Metall. 21 (1973) 571–574. doi:10.1016/0001-6160(73)90064-3.
[43] H.J. Böhm, S. Nogales, Mori–Tanaka models for the thermal conductivity of composites with interfacial resistance and particle size distributions, Compos. Sci. Technol. 68 (2008) 1181–1187. doi:10.1016/j.compscitech.2007.06.009.
[44] W.R.L. da Silva, J. Němeček, P. Štemberk, Application of multiscale elastic homogenization based on nanoindentation for high performance concrete, Adv. Eng. Softw. 62–63 (2013) 109–118. doi:10.1016/j.advengsoft.2013.04.007.
[45] S. Das, P. Yang, S.S. Singh, J.C.E. Mertens, X. Xiao, N. Chawla, N. Neithalath, Effective properties of a fly ash geopolymer: Synergistic application of X-ray synchrotron tomography, nanoindentation, and homogenization models, Cem. Concr. Res. 78, Part B (2015) 252–262. doi:10.1016/j.cemconres.2015.08.004.
[46] L. Sorelli, G. Constantinides, F.-J. Ulm, F. Toutlemonde, The nano-mechanical signature of Ultra High Performance Concrete by statistical nanoindentation techniques, Cem. Concr. Res. 38 (2008) 1447–1456. doi:10.1016/j.cemconres.2008.09.002.
[47] C.C. Yang, APPROXIMATE ELASTIC MODULI OF LIGHTWEIGHT AGGREGATE, Cem. Concr. Res. 27 (1997) 1021–1030. doi:10.1016/S0008-8846(97)00099-9.
[48] H. Hiroshi, T. Minoru, Equivalent inclusion method for steady state heat conduction in composites, Int. J. Eng. Sci. 24 (1986) 1159–1172. doi:10.1016/0020-7225(86)90011-X.
[49] Y. Benveniste, On the effective thermal conductivity of multiphase composites, Z. Für Angew. Math. Phys. ZAMP. 37 (1986) 696–713. doi:10.1007/BF00947917.
[50] P. Meshgin, Y. Xi, Multi-scale composite models for the effective thermal conductivity of PCM-concrete, Constr. Build. Mater. 48 (2013) 371–378. doi:10.1016/j.conbuildmat.2013.06.068.
[51] L.N. McCartney, A. Kelly, Maxwell's far-field methodology applied to the prediction of properties of multi-phase isotropic particulate composites, Proc. R. Soc. Lond. Math. Phys. Eng. Sci. 464 (2008) 423–446. doi:10.1098/rspa.2007.0071.
[52] C.F. Dunant, B. Bary, A.B. Giorla, C. Péniguel, J. Sanahuja, C. Toulemonde, A.-B. Tran, F. Willot, J. Yvonnet, A critical comparison of several numerical methods for computing effective properties of

highly heterogeneous materials, Adv. Eng. Softw. 58 (2013) 1–12. doi:10.1016/j.advengsoft.2012.12.002.
[53] M.I. Idiart, F. Willot, Y.-P. Pellegrini, P. Ponte Castañeda, Infinite-contrast periodic composites with strongly nonlinear behavior: Effective-medium theory versus full-field simulations, Int. J. Solids Struct. 46 (2009) 3365–3382. doi:10.1016/j.ijsolstr.2009.05.009.
[54] S. Das, A. Maroli, S.S. Singh, T. Stannard, X. Xiao, N. Chawla, N. Neithalath, A microstructure-guided constitutive modeling approach for random heterogeneous materials: Application to structural binders, Comput. Mater. Sci. 119 (2016) 52–64. doi:10.1016/j.commatsci.2016.03.040.